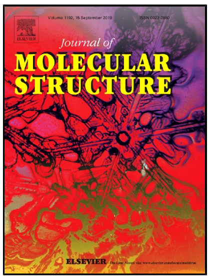

Synthesis and determination of fluorescence properties of new soluble diketopyrrolopyrrole type photosensitizers

Sevil türkçen, Haluk dinçalp, Gözde murat saltan

PII: S0022-2860(19)30735-5

DOI: 10.1016/j.molstruc.2019.06.022

Reference: MOLSTR 26664

To appear in: *Journal of Molecular Structure*

Received Date: 24 February 2019

Accepted Date: 05 June 2019

Please cite this article as: Sevil türkçen, Haluk dinçalp, Gözde murat saltan, Synthesis and determination of fluorescence properties of new soluble diketopyrrolopyrrole type photosensitizers, *Journal of Molecular Structure* (2019), doi: 10.1016/j.molstruc.2019.06.022

Synthesis and determination of fluorescence properties of new soluble diketopyrrolopyrrole type photosensitizers

Sevil TÜRKÇEN[1], **Haluk DİNÇALP**[1*], **Gözde MURAT SALTAN**[1]

[1]Department of Chemistry, Faculty of Arts and Science, Manisa Celal Bayar University, Yunus Emre, 45140 Manisa, Turkey

* Corresponding author e-mail: haluk.dincalp@cbu.edu.tr (H. Dinçalp); Tel: +90 236 2013158; Fax: +90 236 2412158

Abstract: Four organic small molecules bearing phenyl diketopyrrolopyrrole (DPP) unit as the main acceptor group and indole as the main thermal group with soluble units, coded as **DPP3(a-b**) and **DPP4(a-b)**, were synthesized and their optical/electrochemical properties were investigated. Intense visible absorption bands around 480 nm were assigned to the DPP main core, as well as bands around 600 nm were attributed to the formation of charge-transfer complex between the electron-rich indole units and electron-withdrawing DPP core in chloroform solution. All of the compounds were found to be fluorescent in solution and on thin films with emission wavelengths between 500 and 700 nm. The fluorescence decay kinetic measurements of these dyes were also studied. The synthesized compounds have electrochemical energy band gaps from 2.15 to

2.28 eV. Then, the potential usage of the final products in bulk heterojunction solar cells (BHJ-OSCs) were evaluated.

Key words: Diketopyrrolopyrrole, indole, charge transfer, decay time, organic solar cell

1. Introduction

Since the first synthesis of DPP chromophore described by Farnum et al. in 1974 [1] as an original dye for painting and ink industries, [2] these chromophores have found great applications in many areas such as organic field effect transistors (OFETs), [3-6] organic solar cells, [7-12] organic light emitting diodes (OLEDs), [13, 14] fluorescent sensors, [15] photodetectors, [16] biological molecular probes, [17] and photodynamic therapy [18] etc. Because of their many advantages such as their bright colors, excellent stabilities, high mobility values, high fluorescence quantum yields, broad absorption ranges in visible region, two-photon absorption activities and simple synthesis/modification procedures, [2, 19-23] DPP dyes attracted great attention especially in organic electronics.

DPP has a planar structure and shows molecular packing due to strong intermolecular H-bonding between the amide hydrogen atoms and neighboring heteroatoms. [2, 15] This type re-organization of the molecules is responsible for the remarkable red-shifts of the absorption bands to the wavelength beyond 540 nm. Furthermore, the solubility problem of DPP-based dyes can be overcome by attaching long alkyl chains to the nitrogen atoms of amide side of the molecule.

[24, 25] The charge transfer possibility and photo-electron injection ability of DPP dyes can be improved by extending π-conjugation and optimizing the organization of the molecules on substrate surface. [26-30] DPP-based molecules posses good field-effect transistor performance values recorded at 0.7 $cm^2V^{-1}cm^{-1}$ [31] for hole mobility and 0.96 $cm^2V^{-1}cm^{-1}$ [32] for electron mobility.

In the field of BHJ-OSCs, remarkable power conversion efficiencies (PCEs) have been obtained by the challenging DPP structures in both polymer and also small molecule designs. Since the first reports on the photovoltaic performances in solar photovoltaics for polymer and small molecule DPPs by Nguyen [33] and Janssen, [34] respectively, DPP-based polymer structures get the highest PCE value around 9.4% as the donor material. [35] Up to date, the PCE for the small molecule DPP donor structure catched the notable value at 8%. [36] DPP derivatives have also been preferred as acceptor component in the active layer of BHJ-OSCs with the high PCE of 5.1% in the literature. [37] Recently, DPP-based small molecules with different molecular arrangements gave promising efficiencies in solar cells. Thin film quality and suitable morphology of the molecules depend on the molecular packing and crystallinity of DPP molecules, which will be crucial effect on photovoltaic performance. Molecular shape and chain length of solubilizing alkyl groups have remarkable effect on molecular packing of DPP structures. [12] In addition, energy levels and optical properties of DPP molecules can be easily varied by the formation of intramolecular charge transfer (ICT) complex between the acceptor and donor sites of the structure.

Incorporation of donor subunits such as indole with suitable solubilizing groups on the main DPP core may be good combination for promising dye molecule for BHJ-OSC device. In the present work, four different small molecules coded as **DPP3(a-b)** and **DPP4(a-b)** were designed and synthesized (Scheme 1). The effects of extending π-conjugated indole groups on the absorption, emission and redox changes of the DPP cores were investigated. The main purpose of this study is to provide a detailed spectroscopic data for these new DPP dyes which will be focused on the photovoltaic responsibilities.

Scheme 1 [38-41]

2. Experimental

2.1. General

The main reagents used for the synthesis of DPP dyes, 4-bromobenzonitrile, sodium, Iron(III) chloride, diethyl succinate, 5-indolylboronic acid, N-Boc-indole-2-boronic acid, 2-ethylhexyl bromide, di-*tert*-butyl dicarbonate, 4-(dimethylamino)pyridine were purchased from Sigma Aldrich. *Tetrakis*(triphenylphosphine)palladium(0) ($Pd(PPh_3)_4$) catalyst was purchased from TCI company. [6,6]-Phenyl C_{61}-butyric acid methyl ester (PCBM), poly(3-hexylthiophene-2,5-diyl) (P3HT), were purchased from Adrich. All other chemicals and solvents were purchased from Merck, and used without further purification. The purification and isolation of the products were performed by column chromatography on silica gel 60 (0.060-0.200 mm).

^1H NMR and ^{13}C NMR spectra were recorded using a Bruker 400 MHz spectrometer with tetramethylsilane (TMS) as the internal reference, and their chemical shifts were recorded in ppm values. FT-IR spectra were recorded on a Perkin Elmer-Spectrum BX spectrophotometer preparing KBr pellets. UV–vis absorption spectra were recorded on a Perkin Elmer Lambda 950 spectrophotometer. The fluorescence emission of DPP dyes have been measured by using FLS 920 Edinburg instrument. Single photon counting measurements have been taken at the excitation wavelength of 472.4 nm on an apparatus described elsewhere. [42] Fluorescence decays were analyzed globally using exponential tail fit method. [43] Fluorescence decay data were collected at $\lambda_{detection}$ = 520 nm for the dyes. The quality of the fits has been judged by the fitting parameters such as $\chi^2 \leq 1.2$. [44] PL quenching experiments were performed on a Perkin Elmer LS 55 Luminescence Spectrometer. Cyclic voltammetry (CV) measurements of compounds DPP dyes in MeCN solution were measured using 100 mM [TBA][PF_6] as the electrolyte in a CH instruments 660B-Electrochemical Workstation at a scan rate of 100 mV/s. Ferrocene was used as the internal standard and its oxidation potential was detected at +0.53 V. A standard three-electrode configuration cell composed of a platinum wire auxiliary electrode, a glassy carbon working electrode, and an Ag/Ag^+ reference electrode (SCE) was used to measure the oxidation and reduction potentials of the target compounds. The HOMO and LUMO energy levels were calculated from the CV measurements using the given equations below: [45]

$$E_{HOMO} = -e\left(E_{ok}^{onset} + 4.8\right); \qquad E_{LUMO} = -e\left(E_{ind}^{onset} + 4.8\right)$$

$$E_g^{opt} = \frac{1240}{\lambda_{abs}^{onset}}; \qquad E_{LUMO} = E_{HOMO} - E_g^{opt}$$

2.1. Synthesis

2.1.1. Synthesis of 3,6-*Bis*(4-bromophenyl)-2,5-dihydropyrrolo[3,4-c]pyrrole-1,4-dione (DPP1)

Sodium metal (75 mg, 3.26 mmol) was dissolved in *tert*-amyl alcohol (10 mL), and then trace amounts of $FeCl_3$ were added. The mixture was refluxed under an argon atmosphere at 100 ^oC until the solution became clear. 4-bromobenzonitrile (0.5 g, 2.75 mmol) and diethyl succinate (0.24 g, 1.38 mmol) were added to this solution. The mixture was refluxed at 120 °C for 2 h, and then stirred at room temperature for 24 h. The resulting mixture poured into 20 mL of distilled water. The resulting red-colored solids were filtered. The solids were washed with cold MeOH and warm MeOH, respectively, finally dried in the oven.

Yield 75%, FT-IR (KBr pellet, cm^{-1}): 3141 (aromatic $\nu_{C\text{–}H\ \text{stretching}}$), 1639 ($\nu_{C=O}$), 1603 (aromatic $\nu_{C=C}$), 1493, 1438, 1323, 1193, 1140, 1072, 1009, 817, 752, 695 cm^{-1}. ^1H NMR (400 MHz, DMSO-d_6 δ 2.48 ppm): δ = 7.71-7.85 (8H, multiplet) ppm.

2.1.2. Synthesis of 3,6-*Bis*(4-bromophenyl)-2,5-bis[(2S)-2-ethylhexyl]-2,5-dihydropyrrolo[3,4-c]pyrrole-1,4-dione (DPP2a)

To a solution of **DPP1** (50 mg, 0.11 mmol) in NMP (1.5 mL) were added potassium carbonate (62 mg, 0.45 mmol) and 2-ethylhexyl bromide (64 mg, 0.33 mmol). After addition, the mixture was refluxed for 24 h at 100 °C under an argon atmosphere. After completion, the mixture was poured into 20 mL of water, and then extracted with dichloromethane (3×20 mL). The collected organic phases were dried over $MgSO_4$, and then evaporated. The product mixture was purified by column chromatography on silica gel eluting with *n*-hexane:ethylacetate (4: 1).

Yield 60 %, FT-IR (KBr pellet, cm^{-1}): 2957, 2923 ve 2851 (aliphatic $\nu_{C–H\ stretching}$), 1723 ($\nu_{C=O}$), 1590 (aromatic $\nu_{C=C}$), 1463, 1384 1271, 1115, 1012, 824 cm^{-1}. ^{1}H NMR (400 MHz, $CDCl_3$ δ 7.26 ppm): δ = 7.89 (4H, d, *J* = 8.5 Hz), 7.57 (4H, d, *J* = 8.5 Hz), 4.24 (2H, d, *J* = 1.7 Hz), 4.23 (2H, d, *J* = 1.7 Hz), 2.00-2.07 (2H, m), 1.25-1.30 (16H, m), 0.88-0.94 (12H, m) ppm. ^{13}C NMR (100 MHz, $CDCl_3$ δ 77.1 ppm): δ = 166.3, 132.4, 131.9, 131.3, 130.3, 128.1, 115.4, 67.8, 39.2, 30.8, 29.2, 24.1, 23.3, 14.3, 11.3 ppm.

2.1.3. Synthesis di-*tert*-butyl 3,6-*bis*(4-bromophenyl)-1,4-dioxopyrrolo[3,4-c]pyrrole-2,5(1H,4H)-dicarboxylate (DPP2b)

A 25 mL of Schlenk tube was charged with **DPP1** (50 mg, 0.11 mmol), 4-(dimethylamino)pyridine (DMAP) (20 mg, 0.16 mmol), di-*tert*-butyldicarbonate (22 mg, 0.10 mmol), and THF (8 mL). After addition, the mixture was stirred for 24 h at room temperature under an argon atmosphere.The crude product was purified by flash chromatography using toluene:ethylacetate (4:1) as eluent, and the solvent was removed in vacuo to obtain the pure product.

Yield 70%, FT-IR (KBr pellet, cm^{-1}): 2968 ve 2920 (aliphatic $\nu_{C–H\ stretching}$), 1754 (ester $\nu_{C=O}$), 1716 (amide $\nu_{C=O}$), 1600 (aromatic $\nu_{C=C}$), 1484, 1395, 1371, 1279, 1260, 1213, 1153, 1115, 1058, 889, 860 cm^{-1}. ^{1}H NMR (400 MHz, $CDCl_3$ δ 7.28 ppm): δ = 7.61-7.65 (8H, multiplet), 1.45 (18H, s) ppm. ^{13}C NMR (100 MHz, $CDCl_3$ δ 76.9 ppm): δ = 159.0, 147.9, 145.2, 130.4, 129.8, 126.9, 126.2, 112.5, 85.7, 27.6 ppm.

2.1.4. General method for Suzuki-Miyaura coupling reactions

In a Schlenk flask, the Ar-X (1.00 eq.), potassium carbonate (2.00 eq.) and the boronic acid (3.50 eq.) were set under inert atmosphere by three vaccum/argon cycles. Then, the corresponding solvent, toluene (typically 10 mL), and trace amounts of $Pd(PPh_3)_4$ were added. The mixture was degassed by bubbling an argon through and heated to 65 ^{o}C overnight. The residue was purified by column chromatography eluting with toluene:ethyl acetate (4:1) to give the desired product.

2.1.5. Synthesis of 2,5-*Bis*[(2S)-2-ethylhexyl]-3,6-*bis*[4-(1H-indol-5-yl)phenyl]-2,5-dihydropyrrolo[3,4-c]pyrrole-1,4-dione (DPP3a) and Di-*tert*-butyl-3,6-bis[4-(1H-indol-5-yl)phenyl]-1,4-dioxopyrrolo[3,4-c]pyrrole-2,5 (1H,4H)-dicarboxylate (DPP3b)

Both **DPP3a** and **DPP3b** were prepared according to general procedure, starting from the materials **DPP2a** and **DPP2b**, respectively. The boronic acid derivative used in the syntheses was 5-indolylboronic acid.

For DPP3a: Yield 50%, FT-IR (KBr pellet, cm^{-1}): 3412 ($\nu_{\text{N–H stretching}}$), 2957, 2924 ve 2851 (aliphatic $\nu_{\text{C–H stretching}}$), 1712 ($\nu_{C=O}$), 1604 (aromatic $\nu_{C=C}$), 1455, 1413, 1334, 1277, 1245, 1091, 1009, 742 cm^{-1}. ^{1}H NMR (400 MHz, $CDCl_3$ δ 7.25 ppm): δ = 8.26 (2H, s), 8.10 (2H, d, J = 8.6 Hz), 7.91 (1H, s), 7.86 (1H, s), 7.72 (2H, d, J = 8.6 Hz), 7.65 (2H, d, J = 9.6 Hz), 7.41-7.48 (8H, multiplet), 6.63 (2H, d, J = 9.6 Hz), 4.27 (2H, d, J = 3.4 Hz), 4.25 (2H, d, J = 3.4 Hz), 1.72-1.77 (2H, m), 1.25-1.35 (16H, m), 0.98-0.85 (12H, m) ppm. ^{13}C NMR (100 MHz, $CDCl_3$

δ 76.8 ppm): δ = 163.6, 156.7, 150.2, 133.3, 129.9, 128.6, 127.4, 127.0, 126.1, 124.6, 122.0, 116.1, 111.2, 107.4, 103.1, 67.1, 38.9, 30.6, 29.8, 23.8, 22.8, 14.0, 11.0 ppm.

For DPP3b: Yield 60%, FT-IR (KBr pellet, cm^{-1}): 3333 ($\nu_{\text{N–H stretching}}$), 2957, 2918 ve 2851 (aliphatic $\nu_{\text{C–H stretching}}$), 1753 (ester $\nu_{\text{C=O}}$), 1672 (amide $\nu_{\text{C=O}}$), 1602 (aromatic $\nu_{\text{C=C}}$), 1471, 1367, 1281, 1253, 1146, 1107, 1060, 802 cm^{-1}. ^{1}H NMR (400 MHz, $CDCl_3$ δ 7.26 ppm): δ = 8.32 (2H, s), 7.88 (2H, d, J = 7.7 Hz), 7.74 (4H, d, J = 6.4 Hz), 7.71 (4H, d, J = 6.4 Hz), 7.62 (2H, s), 7.42-7.50 (2H, m), 7.28 (2H, d, J = 9.6 Hz), 6.64 (2H, d, J = 9.6 Hz), 1.45 (18H, s) ppm. ^{13}C NMR (100 MHz, $CDCl_3$ δ 76.8 ppm): δ = 169.0, 159.4, 149.7, 146.9, 135.9, 132.4, 131.3, 129.8, 127.8, 125.2, 121.4, 119.6, 119.3, 111.5, 109.7, 103.2, 84.1, 27.5 ppm.

2.1.6. Synthesis of Di-*tert*-butyl 2,2'-[{2,5-*bis*[(2S)-2-ethylhexyl]-3,6-dioxo-2,3,5,6-tetrahydropyrrolo[3,4-c]pyrrole-1,4-diyl}*bis*(4,1-phenylene)]*bis*(1H-indole-1-carboxylate) (DPP4a) and Di-*tert*-butyl 3,6-*bis*{4-[1-(*tert*-butoxycarbonyl)-1H-indol-2-yl]phenyl}-1,4-dioxopyrrolo[3,4-c]pyrrole-2,5(1H,4H)-dicarboxylate (DPP4b)

Compound **DPP4a** and **DPP4b** were synthesized following the general prosedure, starting from the materials **DPP2a** and **DPP2b**, respectively. The boronic acid derivative used in the syntheses was N-Boc-indole-2-boronic acid.

For DPP4a: Yield 40%, FT-IR (KBr pellet, cm^{-1}): 2957, 2929, 2862 (aliphatic $\nu_{\text{C–H stretching}}$), 1734 ($\nu_{\text{C=O}}$), 1605 ($\nu_{\text{C=O}}$), 1451, 1337, 1251, 1160, 1119, 1023, 850, 746 cm^{-1}. ^{1}H NMR (400 MHz, $CDCl_3$ δ 7.29 ppm): δ = 8.04 (2H, s), 7.87 (2H, s), 7.61 (2H, s), 6.94-7.04 (10H, m), 6.36 (2H, s), 3.95 (2H, broad), 3.75 (2H, broad), 2.22-2.35 (2H, m), 1.39 (18H, s), 0.96-1.14 (16H, m), 0.62 (12H, broad) ppm. ^{13}C NMR (100 MHz, $CDCl_3$ δ 77.1 ppm): δ = 165.9, 157.6, 149.7, 131.7, 131.0, 128.7, 125.7, 124.7, 124.0, 122.7, 122.5, 120.9, 115.5, 115.1, 111.2, 107.2, 83.2, 67.7, 38.8, 30.5, 29.7, 28.1, 27.7, 22.9, 13.9, 11.0 ppm.

For DPP 4b: Yield 45%, FT-IR (KBr pellet, cm^{-1}): 3054, 2979, 2933 (aliphatic $\nu_{\text{C–H stretching}}$), 1733 ($\nu_{C=O}$), 1608 (amide $\nu_{C=O}$), 1595 (aromatic $\nu_{C=C}$), 1452, 1369, 1335, 1252, 1159, 1134, 1025, 851, 747 cm^{-1}. ^{1}H NMR (400 MHz, $CDCl_3$ δ 7.26 ppm): δ =8.17 (2H, dd, J_1 = 12.1, J_2 = 6.5 Hz), 7.67 (4H, d, J = 8.6 H), 7.49-7.55 (6H, m), 7.35 (2H, dd, J_1 = 12.1, J_2 = 6.5 Hz), 7.23 (2H, d, J = 8.6 Hz), 6.64 (2H, s), 1.37 (18H, s), 1.33 (18H, s) ppm. ^{13}C NMR (100 MHz, $CDCl_3$ δ 76.9 ppm): δ = 169.0, 159.1, 156.0, 139.4, 138.3, 137.6, 132.0, 131.5, 129.2, 128.9, 125.1, 123.3, 120.8, 118.8, 115.4, 111.7, 111.0, 84.6, 84.1, 27.7, 27.6 ppm.

3. Results and Discussion

3.1. Optical properties and time resolved measurements

Diethylsuccinate in *tert*-AmOH is condensed with 4-bromobenzonitrile using metalic sodium to afford the desired product **DPP1** via pseudo-Stobbe condensation pathway. [46] In order to increase the solubility of this dye, **DPP2a** and **DPP2b** derivatives substituted with ethylhexyl and di-*tert*-butyl dicarbonate groups at the 2, 5-positions of the DPP moiety were synthesized, respectively. Then, **DPP3a**, **DPP3b**, **DPP4a** and **DPP4b** were prepared by $Pd(PPh_3)_4$ assisted Suzuki coupling reaction of **DPP2a** and **DPP2b** with 5-indolylboronic acid, N-Boc-indole-2-boronic acid, respectively. The chemical structures and purity of all compounds were identified by FT-IR, ^{1}H-NMR, ^{13}C-NMR. In the FT-

IR spectrum of **DPP2b**, **DPP3b**, **DPP4a** and **DPP4b**, the typical ester C=O stretch band between 1733 and 1754 cm^{-1} was taken as the evidence of the attachment of Boc group the main core. The ^{1}H NMR spectra of indole-substituted **DPP3(a-b)** and **DPP4(a-b)** dyes are compatible with the proposed structures. The ^{1}H NMR spectrum of heteroaromatic side of the structures showed slightly remarkable up-field shifts around 6.64 ppm in which indicated the indole aromatic C−H bond.

Figure 1a

Figure 1b

Fig. 1a gives the comparison of the normalized UV−vis absorption spectra of **DPP3(a-b)** and **DPP4(a-b)** dyes in chloroform solution, and the corresponding optical properties are summarized in Table 1. In the studied solvents, **DPP3(a-b)** and **DPP4(a-b)** dyes give broad absorption bands within the range of 457-486 nm wavelength in which were assigned to the localized π–π^* transitions. These absorptions were attributed to the loss of the H-bonding capability of DPP core because of the distorted molecular packing system for pyrrole rings initiated by N-substitution with Boc or ethylhexyl groups. Similar short-wavelength absorption values were observed for Boc-protected derivatives of DPP molecules in the previous studies. When the protected groups are released from the nitrogen atom, $\lambda_{\max}$ values for all DPP structures are shifted to the wavelength above 540 nm. [38, 47] The absorption bands in much higher energy states could be generated to from the specific aromatic sides of the structures.

Comparison of the normalized UV–vis absorption spectra of **DPP3a** dye in different solvents and, also on thin film is given in Fig. 1b. The most striking observation is the appearance of low-lying broad band around 600 nm for **DPP3(a-b)** and **DPP4(a-b)** dyes in chloroform solution. Noting that this observation is corresponded to the ICT transition between the DPP core and indole units, known from the literature. [48, 49] Interestingly, this red-shift in $\lambda_{\max}$ value was not observed in more polar MeCN solution. Also, the absorption maximum of all dyes are slightly shifted to blue region in MeCN solution. Both observations are more consistent with much lower polarizability of the excited dye with respect to its ground state in MeCN solution, which then heightens the LUMO energy level of the studied dyes. This hampers the charge transfer from indole group to the central DPP side. As can be seen from Table 1 that absorption maximum of **DPP3a** and **DPP4a** dyes are more shifted to red region as compared to that of **DPP3b** and **DPP4b** in the studied solvents. Because ethylhexyl groups contribute to ring resonance by giving their electrons to the nitrogen atom of DPP core through sigma bonds. Also, compared to the absorption spectra in solution, these ones in the solid state have slightly red-shifted (around 4-19 nm) indicating that π–π^* interaction due to molecular packaging existed in the solid state.

Figure 2a

Figure 2b

Table 1

The fluorescence emission spectra of **DPP3(a-b)** and **DPP4(a-b)** dyes in chloroform are plotted as shown in Fig. 2a. DPP core shows mainly two emission regions when excited at 485 nm. Emission bands are observed between 514 and 598 nm and their maximas are changed according to the polarity of the used solvents and the attached groups. The emission maxima of **DPP3a** dye slightly shifts more red region when compared the other dyes in the studied solvents. Comparison of fluorescence emission spectra of **DPP3a** and **DPP4a** dyes coated on thin films are also shown in Fig. 2b. The thin films show similar emission profiles, but emission maxima on thin films displays slightly larger red-shifts as compared to that of solution phases.

Figure 3a

Figure 3b

Fig. 3a compares the fluorescence emission spectra of DPP core with its indole subunit for **DPP3a** dye in chloroform solution by changing the setting of excitation wavelength from 260 to 540 nm. When we excite the sample at the wavelengths between 260 and 340 nm in which mainly indole can absorb, the emission peak of indole fragment was located around 400 nm (0–0). At this situation, emission of DPP part of the structure seems to arise from the energy transfer between the excited indole and DPP core. The absorption spectrum of acceptor DPP group could overlap partially with the fluorescence emission spectrum of indole donor, as a result resonance energy transfer occurs in the structure of **DPP3a** dye to generate DPP emission signal. As the excitation wavelengths approach to the DPP absorption region, the fluorescence spectra show only one broad emission signal belonging to the DPP core. We could not detect any emission signals beyond the excitation wavelength of 540 nm due to limitations of the optical absorptions of the studied dyes in this region. Fig. 3b displays the excitation spectrum of all dyes in chloroform solution at the collected emission wavelength of 520 nm. Excitation spectrum is very well-matched with the absorption profile of the dyes as illustrated in Fig. 1a excluding ICT absorption. Noting that the collected emission signal were generated from the DPP absorption profile as described above.

Figure 4

Fig. 4 shows the fluorescence decay of **DPP3a** in chloroform solution at detection wavelength of 520 nm. Analysis of the decays revealed mono-exponential decays for all dyes in chloroform and acetonitrile as given in Table 1. Fluorescence lifetimes of all dyes were calculated with the range of 2.79–6.63 ns depending on the structure of the dyes and used solvents.

3.2. CV measurements and PL quenching studies

For getting better efficiencies from BHJ-OSCs in which organic dyes are used in their photoactive layer, the energy levels of the dyes must be compatible with each other and also metal electrodes to achieve efficient electron transfer. In order to clarify the efficient electron transfer, the HOMO/LUMO energy levels including electrochemical band gaps of all dyes were determined from the electrochemical measurements with cyclic voltammetry. The reduction and oxidation voltammograms of all dyes on glassy carbon working electrode in 0.1M [TBA][PF_6]/Me-CN are illustrated in Fig. 5(a-b) and their electrochemical data are summarized in Table 2. While compounds **DPP4(a-b)** exhibit two reduction waves and two oxidation waves, while compounds **DPP3(a-b)** exhibit one reduction-oxidation wave. The HOMO energy levels of all dyes range from −5.45 eV and −5.79 eV, and the LUMO energy levels of **DPP3(a-b)** and **DPP4(a-b)** are calculated to be about −3.45, −3.57 eV, and −3.51, −3.22 eV, respectively.

Figure 5a

Figure 5b

Table 2

Fast photoinduced charge transport from donor to acceptor is very essential issue for an effective BHJ-OSC devices. In order to analyze the charge transfer possibilities between the synthesized dyes and organic photovoltaic materials such as P3HT and PCBM in device structure, we report PL quenching of P3HT polymer donor by **DPP3b** dye and, also all dyes by PCBM acceptor.

The solution of 4.2×10^{-4} M **DPP3b** dye was prepared in THF and at each addition 20 μL of this solution was poured into the 2.7 mL THF solution of 1.1×10^{-6} M P3HT which was placed in a quartz cuvette. After each addition, change in fluorescence intensity of P3HT was followed. Fig. 6 revealed that the PL peak intensity of pristine P3HT (λ_{exc}=440 nm) increased dramatically by the addition of **DPP3b** dye over the concentration starting from 3.1×10^{-6} M to 76.4×10^{-6} M. This increase can be due to 440 nm excitation also exciting **DPP3b** dye, and it can also be attributed to the additional emission integral of the emissive **DPP3b** dye. Then, PL quenching studies were repeated using dye:PCBM system to analyze the charge transfer possibilities. PL quenching experiments were performed by the addition of 4.2×10^{-4} M THF solution of PCBM into the 2.7 mL

THF solutions of ~3×10^{-6} M **DPP3(a-b)** and **DPP4(a-b)** dyes. After each addition of 20 μL of PCBM solution, dyes were excited at 485 nm to get much better PL signal. Fig. 7(a-d) revealed that the PL peak intensity of each pristine dyes decreased dramatically over the increasing PCBM concentrations. The decrease could be mainly assigned to an efficient charge transfer from the donor dyes to PCBM acceptor. This observation is supported by the appropriate HOMO-LUMO energy levels of PCBM acceptor and synthesized dyes to get better charge injection. It was noted that **DPP3(a-b)** and **DPP4(a-b)** dyes may be used as donor component instead of P3HT donor towards PCBM acceptor in BHJ-OSCs.

Figure 6

Figure 7a

Figure 7b

Figure 7c

Figure 7d

Corresponding Stern-Volmer plots for PL quenching process for **DPP3b**:PCBM and **DPP4b**:PCBM are illustrated in Fig. 8. The Stern-Volmer quenching constants (K_{sv}) for **DPP3b**:PCBM and **DPP4b**:PCBM titrations were found to be about 750.9 $M^{-1}ns^{-1}$ and 1193.5 $M^{-1}ns^{-1}$, respectively. These high quenching rates can be taken as evidences of occurrence electron transfer from diketopyrrolopyrrole dyes to strong acceptor PCBM.

Figure 8

4. Conclusions

In this work, four new small molecules based on linear D-A-D type DPP consisting of different aryl electroactive and different soluble groups were designed and successfully synthesized. All dyes represented an optical band gap of 2.15-2.28 eV with suitable energy levels. According to these values, the calculated LUMO energy levels of the new dyes are above the LUMO energy level of standart PCBM acceptors (~3.9 eV). This indicates that there may be an efficient electron transfer between donor DPP molecule and PCBM acceptor in the BHJ-OSC device charge transfer mechanism. It is advisable that these new dyes can be applicable as a donor component in the photo-active layer of BHJ-OSCs. In conclusion, these results can be an efficient new approach to obtain high performance organic solar cells with improved processability.

Acknowledgments

Financial support for this work was provided by the Research Council of Manisa Celal Bayar University with the project number of 2016-018.

References

[1] D.G. Farnum, G. Mehta, G.G.I. Moore, F.P. Siegal, Attempted reformatskii reaction of benzonitrile, 1,4-diketo-3,6-diphenylpyrrolo[3,4-C]pyrrole. A lactam analogue of pentalene, Tetrahedron Lett. 15(29) (1974) 2549–2552.

[2] B. Tieke, A.R. Rabindranath, K. Zhang, Y. Zhu, Conjugated polymers containing diketopyrrolopyrrole units in the main chain, Beilstein J. Org. Chem. 6 (2010) 830–845.

[3] C.B. Nielsen, M. Turbiez, I. McCulloch, Recent advances in the development of semiconducting DPP-containing polymers for transistor applications, Adv. Mater. 25(13) (2013) 1859–1880.

[4] A.K. Palai, H. Cho, S. Cho, T.J. Shin, S. Jang, S.-U. Park, S. Pyo, Non-functionalized soluble diketopyrrolopyrrole: Simplest p-channel core for organic field-effect transistors, Org. Electron. 14(5) (2013) 1396–1406.

[5] P. Sonar, S.P. Singh, Y. Li, M.S. Soh, A. Dodabalapur, A low-bandgap diketopyrrolopyrrole-benzothiadiazole-based copolymer for high-mobility ambipolar organic thin-film transistors, Adv. Mater. 22(47) (2010) 5409–5413.

[6] Y. Li, P. Sonar, L. Murphy, W. Hong, High mobility diketopyrrolopyrrole (DPP)-based organic semiconductor materials for organic thin film transistors and photovoltaics, Energ. Environ. Sci. 6(6) (2013) 1684–1710.

[7] D. Chandran, K.-S. Lee, Diketopyrrolopyrrole: A versatile building block for organic photovoltaic materials, Macromol. Res. 21(3) (2013) 272–283.

[8] J.C. Bijleveld, V.S. Gevaerts, D. Di Nuzzo, M. Turbiez, S.G. Mathijssen, D.M. de Leeuw, M.M. Wienk, R.A. Janssen, Efficient solar cells based on an easily accessible diketopyrrolopyrrole polymer, Adv. Mater. 22(35) (2010) E242–246.

[9] A.B. Tamayo, X.-D. Dang, B. Walker, J. Seo, T. Kent, T.-Q. Nguyen, A low band gap, solution processable oligothiophene with a dialkylated diketopyrrolopyrrole chromophore for use in bulk heterojunction solar cells, Appl. Phys. Lett. 94(10) (2009) 103301(1–3).

[10] E. Zhou, S. Yamakawa, K. Tajima, C. Yang, K. Hashimoto, Synthesis and Photovoltaic Properties of Diketopyrrolopyrrole-Based Donor–Acceptor Copolymers, Chem. Mater. 21(17) (2009) 4055–4061.

[11] S. Loser, C.J. Bruns, H. Miyauchi, R.P. Ortiz, A. Facchetti, S.I. Stupp, T.J. Marks, A naphthodithiophene-diketopyrrolopyrrole donor molecule for efficient solution-processed solar cells, J. Am. Chem. Soc. 133(21) (2011) 8142–8145.

[12] A. Tang, C. Zhan, J. Yao, E. Zhou, Design of diketopyrrolopyrrole (DPP)-based small molecules for organic-solar-cell applications, Adv. Mater. 29(2) (2017) 1600013.

[13] T. Beyerlein, B. Tieke, S. Forero-Lenger, W. Brütting, Red electroluminescence from a 1,4-diketopyrrolo[3,4-c]pyrrole (DPP)-based conjugated polymer, Synthetic Met. 130(2) (2002) 115–119.

[14] D. Cao, Q. Liu, W. Zeng, S. Han, J. Peng, S. Liu, Diketopyrrolopyrrole-containing polyfluorenes: facile method to tune emission color and improve electron affinity, Macromolecules 39(24) (2006) 8347–8355.

[15] M. Kaur, D.H. Choi, Diketopyrrolopyrrole: brilliant red pigment dye-based fluorescent probes and their applications, Chem. Soc. Rev. 44(1) (2015) 58–77.

[16] J. Qi, J. Han, X. Zhou, D. Yang, J. Zhang, W. Qiao, D. Ma, Z.Y. Wang, Optimization of broad-response and high-detectivity polymer photodetectors by bandgap engineering of weak donor–strong acceptor polymers, Macromolecules 48(12) (2015) 3941–3948.

[17] S. Tang, E.H. Ghazvini Zadeh, B. Kim, N.T. Toomey, M.V. Bondar, K.D. Belfield, Protein-induced fluorescence enhancement of two-photon excitable water-soluble diketopyrrolopyrroles, Org. Biomol. Chem. 15(31) (2017) 6511–6519.

[18] Y. Cai, Q. Tang, X. Wu, W. Si, Q. Zhang, W. Huang, X. Dong, Bromo-substituted diketopyrrolopyrrole derivative with specific targeting and high efficiency for photodynamic therapy, ACS Appl. Mater. Inter. 8(17) (2016) 10737–10742.

[19] F. Ponsot, N. Desbois, L. Bucher, M. Berthelot, P. Mondal, C.P. Gros, A. Romieu, Near-infrared emissive bacteriochlorin-diketopyrrolopyrrole triads: Synthesis and photophysical properties, Dyes Pigments 160 (2019) 747–756.

[20] X. Liu, L. Kong, H. Du, Y. Zhang, J. Zhao, Y. Xie, Synthesis and electrochromic properties of electrochromic polymers based on propylenedioxythiophene, diketopyrrolopyrrole and benzodithiophene units, Org. Electron. 64 (2019) 223–235.

[21] W. Li, L. Wang, H. Tang, D. Cao, Diketopyrrolopyrrole-based fluorescent probes for detection and bioimaging: current progresses and perspectives, Dyes Pigments 162 (2019) 934–950.

[22] K. Nie, S. Xu, X. Duan, H. Shi, B. Dong, M. Long, H. Xu, X.-F. Jiang, Z. Liu, Diketopyrrolopyrrole-doped hybrid FONs as two-photon absorbing and dual-emission fluorescent nanosensors for Hg^{2+}, Sensors Actuat. B-Chem. 265 (2018) 1–9.

[23] Y. Lin, Y. Li, X. Zhan, Small molecule semiconductors for high-efficiency organic photovoltaics, Chem. Soc. Rev. 41(11) (2012) 4245–4272.

[24] H. Lee, H. Han, J. Jeong, H. Kim , D.-I. Song, Y. Kim, Broadband-solubility diketopyrrolopyrrole derivative with both polar cyano and nonpolar alkyl groups for stable organic photosensors and diffusion-processed organic solar cells, ChemistrySelect 1(8) (2016) 1716–1722.

[25] H.-Y. Lee, J.-S. Yoo, H.-S. Kwon, J.-K. Oh, J.-H. Choi, Preparation and characterizations of solvent soluble dyes based on dimerized diketo-pyrrolo-pyrrole pigment, Mol. Cryst. Liq. Cryst. 617(1) (2015) 73–81.

[26] H. Shi, Z. Gu, X. Gu, H. Pan, J. Pan, X. Hu, C. Fan, M. Shi, H. Chen, Effect of end-groups on the photovoltaic property of diphenyl substituted diketopyrrolopyrrole derivatives, Synthetic Met. 188 (2014) 66–71.

[27] Y. Chen, Z. Du, W. Chen, L. Han, Q. Liu, M. Sun, R. Yang, Near-infrared response thienoisoindigo-based small molecule for solution-processed bulk-heterojunction solar cells, Synthetic Met. 187 (2014) 24–29.

[28] H.-F. Feng, W.-F. Fu, L. Li, Q.-C. Yu, H. Lu, J.-H. Wan, M.-M. Shi, H.-Z. Chen, Z.a. Tan, Y. Li, Triphenylamine modified bis-diketopyrrolopyrrole molecular donor materials with extended conjugation for bulk heterojunction solar cells, Org. Electron. 15(10) (2014) 2575–2586.

[29] S. Li, J. Yuan, P. Deng, W. Ma, Q. Zhang, A comparative study of diketopyrrolopyrrole and isoindigo based polymers for organic photovoltaic applications, Dyes Pigments 106 (2014) 121–127.

[30] J. Chen, M. Xiao, W. Su, X. Duan, L. Duan, W. Peng, H. Tan, R. Yang, W. Zhu, Synthesis, characterization and photovoltaic properties of two-dimensional conjugated polybenzodithiophene derivatives appending diketopyrrolopyrrole units as side chain, Polym. 55(19) (2014) 4857–4864.

[31] S.L. Suraru, U. Zschieschang, H. Klauk, F. Wurthner, Diketopyrrolopyrrole as a p-channel organic semiconductor for high performance OTFTs, Chem. Commun. 47(6) (2011) 1767–1769.

[32] W.S. Yoon, S.K. Park, I. Cho, J.-A. Oh, J.H. Kim, S.Y. Park, High-mobility n-type organic transistors based on a crystallized diketopyrrolopyrrole derivative, Adv. Funct. Mater. 23(28) (2013) 3519–3524.

[33] A.B. Tamayo, B. Walker, T.-Q. Nguyen*, A Low Band Gap, Solution processable oligothiophene with a diketopyrrolopyrrole core for use in organic solar cells, J. Phys. Chem. C 112(30) (2008) 11545–11551.

[34] M.M. Wienk, M. Turbiez, J. Gilot, R.A.J. Janssen, Narrow-bandgap diketo-pyrrolo-pyrrole polymer solar cells: the effect of processing on the performance, Adv. Mater. 20(13) (2008) 2556–2560.

[35] H. Choi, S.J. Ko, T. Kim, P.O. Morin, B. Walker, B.H. Lee, M. Leclerc, J.Y. Kim, A.J. Heeger, Small-bandgap polymer solar cells with unprecedented short-circuit current density and high fill factor, Adv. Mater. 27(21) (2015) 3318–3324.

[36] R.S. Ashraf, I. Meager, M. Nikolka, M. Kirkus, M. Planells, B.C. Schroeder, S. Holliday, M. Hurhangee, C.B. Nielsen, H. Sirringhaus, I. McCulloch, Chalcogenophene comonomer comparison in small band gap diketopyrrolopyrrole-based conjugated polymers for high-performing field-effect transistors and organic solar cells, J. Am. Chem. Soc. 137(3) (2015) 1314–1321.

[37] J.W. Jung, W.H. Jo, Low-Bandgap Small Molecules as non-fullerene electron acceptors composed of benzothiadiazole and diketopyrrolopyrrole for all organic solar cells, Chem. Mater. 27(17) (2015) 6038–6043.

[38] R. Beninatto, G. Borsato, O. De Lucchi, F. Fabris, V. Lucchini, E. Zendri, New 3,6-bis(biphenyl)diketopyrrolopyrrole dyes and pigments via Suzuki–Miyaura coupling, Dyes Pigments 96(3) (2013) 679–685.

[39] X. Zeng, Z. Li, J. Ren, T. Ge, Z. Zang, Q. Sun, H. Wang, Y. Hao, Low bandgap diketopyrrolopyrrole-based polymers with an asymmetric unit of fluoridated

phenylene-thiophene for efficient polymer solar cells, Synthetic Met. 240 (2018) 30–36.

[40] G. Zhang, L. Wang, X. Cai, L. Zhang, J. Yu, A. Wang, A new diketopyrrolopyrrole (DPP) derivative bearing boronate group as fluorescent probe for fluoride ion, Dyes Pigments 98(2) (2013) 232–237.

[41] S.-i. Kato, T. Matsumoto, M. Shigeiwa, H. Gorohmaru, S. Maeda, T. Ishi-i, S. Mataka, Novel 2,1,3-Benzothiadiazole-based red-fluorescent dyes with enhanced two-photon absorption cross-sections, Chem–Eur. J. 12(8) (2006) 2303–2317.

[42] G.M. Saltan, H. Dinçalp, M. Kıran, C. Zafer, S.Ç. Erbaş, Novel organic dyes based on phenyl-substituted benzimidazole for dye sensitized solar cells, Mater. Chem. Phys. 163 (2015) 387–393.

[43] J.R. Knutson, J.M. Beechem, L. Brand, Simultaneous analysis of multiple fluorescence decay curves - a global approach, Chem. Phys. Lett. 102(6) (1983) 501–507.

[44] M. Zuker, A.G. Szabo, L. Bramall, D.T. Krajcarski, B. Selinger, Delta-function convolution method (DFCM) for fluorescence decay experiments, *Rev. Sci. Instrum.* s 56(1) (1985) 14–22.

[45] J. Pommerehne, H. Vestweber, W. Guss, R.F. Mahrt, H. Bassler, M. Porsch, J. Daub, Efficient 2-layer LEDs on a polymer blend basis, Adv. Mater. 7(6) (1995) 551–554.

[46] A. Iqbal, M. Jost, R. Kirchmayr, J. Pfenninger, A. Rochat, O. Wallquist, The synthesis and properties of 1,4-diketo-pyrrolo[3,4-C]pyrroles, B. Soc. Chim. Belg. 97(8-9) (1988) 615–644.

[47] E.D. Glowacki, H. Coskun, M.A. Blood-Forsythe, U. Monkowius, L. Leonat, M. Grzybowski, D. Gryko, M.S. White, A. Aspuru-Guzik, N.S. Sariciftci,

Hydrogen-bonded diketopyrrolopyrrole (DPP) pigments as organic semiconductors, Org. Electron. 15(12) (2014) 3521–3528.

[48] M. Chandrasekharam, M.A. Reddy, K. Ganesh, G.D. Sharma, S.P. Singh, J.L. Rao, Synthesis and photovoltaic properties of D–A–D type small molecules containing diketopyrrolopyrrole (DPP) acceptor central unit with different donor terminal units, Org. Electron. 15(9) (2014) 2116–2125.

[49] G.D. Sharma, J.A. Mikroyannidis, S.S. Sharma, M.S. Roy, K.R. Justin Thomas, Efficient bulk heterojunction photovoltaic devices based on diketopyrrolopyrrole containing small molecule as donor and modified PCBM derivatives as electron acceptors, Org. Electron. 13(4) (2012) 652–666.

Figure Captions

Scheme 1: Synthesis of targeted DPP compounds. Reagents and conditions: *(i)* metalic Na, anhydrous $FeCl_3$, diethylsuccinate/*tert*-AmOH [38], *(ii)* for **DPP2a**; 2-ethylhexyl bromide, NMP/K_2CO_3; [39] for **DPP2b**; DMAP/THF, [40] *(iii)* 1H-indole-5-yl]boronic acid, 2M K_2CO_3, $Pd(PPh_3)_4$, toluene, 65 °C; [39] *(iv)* 1-Boc-indole-2-boronic acid, 2M K_2CO_3, $Pd(PPh_3)_4$, toluene, 65 °C. [41]

Figure 1. (a) Comparison of the normalized UV–vis absorption spectra of **DPP3(a-b)** and **DPP4(a-b)** dyes in chloroform solution. **(b)** Comparison of the normalized UV–vis absorption spectra of **DPP3a** dye in different solvents and, also on thin film.

Figure 2. (a) Comparison of the normalized fluorescence emission spectra of all DPP dyes in chloroform solution **(b)** Comparison of the normalized fluorescence emission spectra of **DPP3a** and **DPP4a** dyes on thin films (λ_{exc}=485 nm).

Figure 3. (a) Comparison of the fluorescence emission spectra of **DPP3a** dye in chloroform solution with different excitation wavelenghts increasing from 360 to 540 nm ($C_{\mathbf{DPP3a}}$: 3.1×10^{-4} M). **(b)** Normalized excitation spectrum of **DPP3(a-b)** and **DPP4(a-b)** dyes in chloroform solution at the emission wavelength of 520 nm.

Figure 4. Fluorescence decay analysis of **DPP3a** dye in chloroform solution ($\lambda_{detection}$ = 520 nm)

Figure 5. Cyclic voltammograms of **(a) DPP3(a-b)**, and **(b) DPP4(a-b)** dyes on glassy carbon working electrode in 0.1 M [TBA][PF_6]/Me-CN (Scan rate: 100 mV s^{-1}).

Figure 6. PL spectra of P3HT at incresing concentrations of **DPP3b** dye in THF at the excitation wavelength of 440 nm (0 M, 3.1×10^{-6} M, 11.5×10^{-6} M, 19.8×10^{-6} M, 28.0×10^{-6} M, 36.2×10^{-6} M, 44.4×10^{-6} M, 52.5×10^{-6} M, 60.5×10^{-6} M, 68.5×10^{-6} M, 76.4×10^{-6} M).

Figure 7. PL spectra of **(a) DPP3a**, **(b) DPP4a**, **(c) DPP3b** and, **(d) DPP4b** at incresing concentrations of PCBM in THF at the excitation wavelength of 485 nm (0 M, 1.6×10^{-6} M, 6.0×10^{-6} M, 10.4×10^{-6} M, 14.7×10^{-6} M, 19.0×10^{-6} M, 23.2×10^{-6} M, 27.5×10^{-6} M, 31.7×10^{-6} M, 35.9×10^{-6} M).

Figure 8. Stern-Volmer plots of **DPP3b** and **DPP4b** dyes PL quenched by PCBM in THF ($y = 2681x + 0.0034$ R^2:0.976 for **DPP3b**, and $y = 3330x + 0.0019$ R^2:0.995 for **DPP4b**).

Table Captions

Table 1

UV–visible absorption (λ (nm)), emission (λ_{em} (nm)) wavelengths and fluorescence decay times ($\tau_{f(n)}$ (ns)) of all dyes in different solvents and, also on thin films (λ_{exc} = 485 nm, $\lambda_{detection}$ = 520 nm).

Table 2

Electrochemical values and HOMO-LUMO energies of **DPP3(a-b)** and **DPP4(a-b)** dyes with respect to the vacuum level.

Research Highlights

1. ICT was observed between the indole donor and the DPP core acceptor.
2. High quenching rates can be taken as evidence of electron transfer.
3. Synthesized dyes can be used as donor component in BHJ-OSCs.

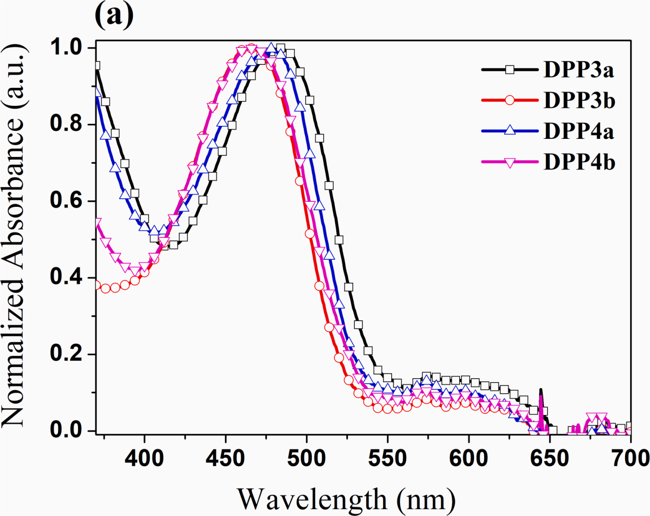
(a)
Normalized Absorbance (a.u.)
1.0
0.8
0.6
0.4
0.2
0.0
400
450
500
550
600
650
700
Wavelength (nm)
DPP3a
DPP3b
DPP4a
DPP4b

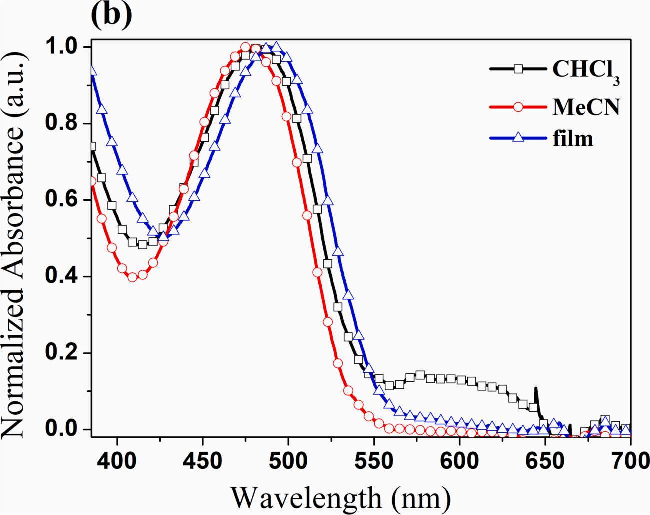
(b)
Normalized Absorbance (a.u.)
0.0
0.2
0.4
0.6
0.8
1.0
400
450
500
550
600
650
700
Wavelength (nm)
CHCl$_3$
MeCN
film

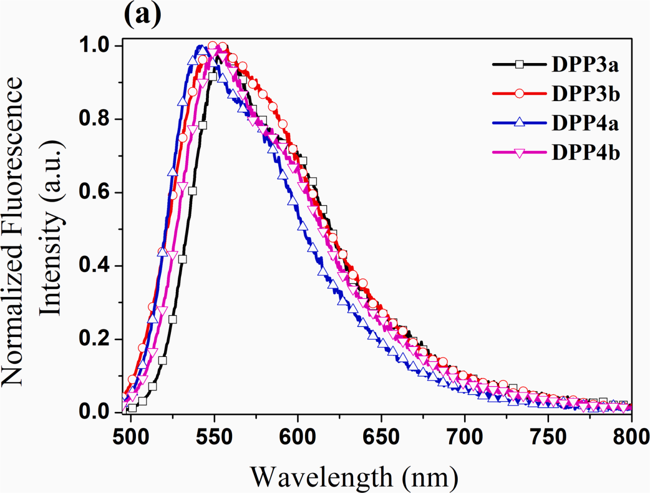
(a)
Normalized Fluorescence Intensity (a.u.)
Wavelength (nm)
DPP3a
DPP3b
DPP4a
DPP4b
0.0
0.2
0.4
0.6
0.8
1.0
500
550
600
650
700
750
800

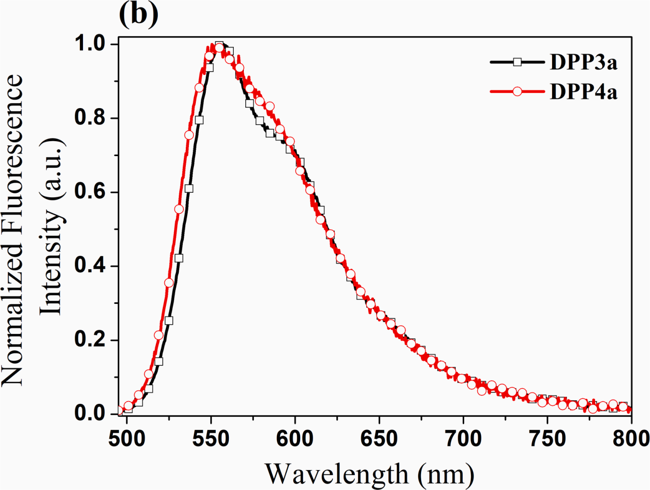
(b)
Normalized Fluorescence Intensity (a.u.)
Wavelength (nm)
DPP3a
DPP4a
0.0
0.2
0.4
0.6
0.8
1.0
500
550
600
650
700
750
800

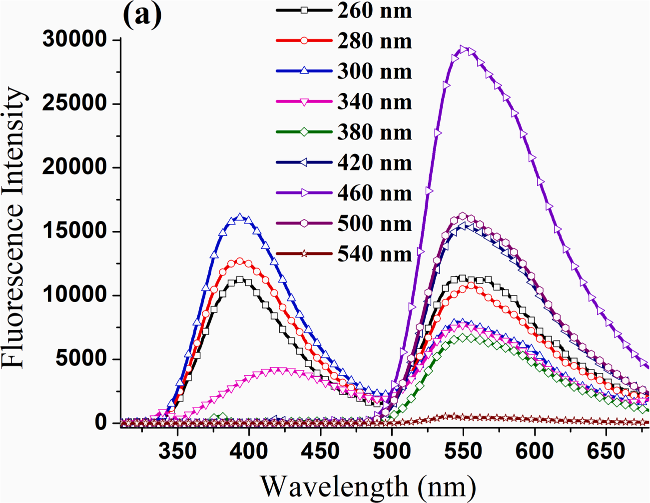
(a)
260 nm
280 nm
300 nm
340 nm
380 nm
420 nm
460 nm
500 nm
540 nm
Fluorescence Intensity
0
5000
10000
15000
20000
25000
30000
Wavelength (nm)
350
400
450
500
550
600
650

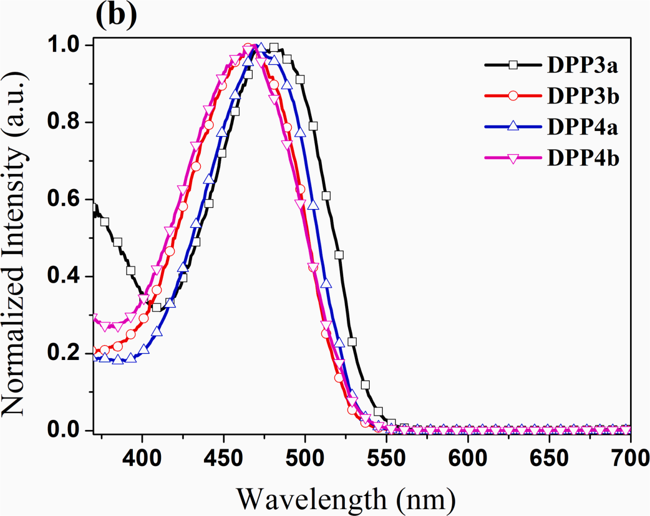
(b)
DPP3a
DPP3b
DPP4a
DPP4b
Normalized Intensity (a.u.)
Wavelength (nm)
0.0
0.2
0.4
0.6
0.8
1.0
400
450
500
550
600
650
700

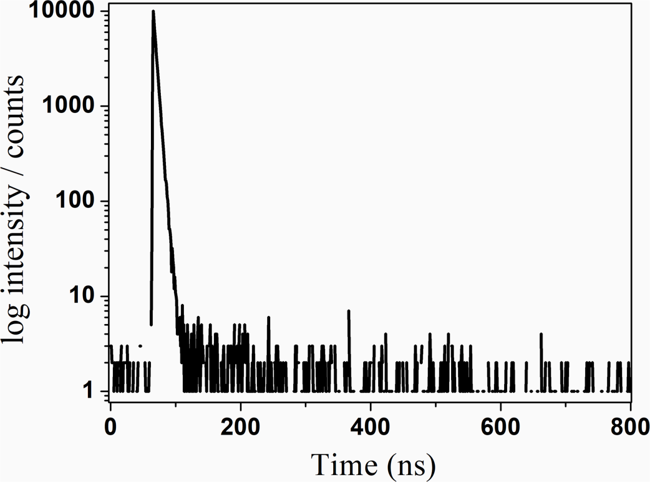
10000
1000
100
10
1
log intensity / counts
0
200
400
600
800
Time (ns)

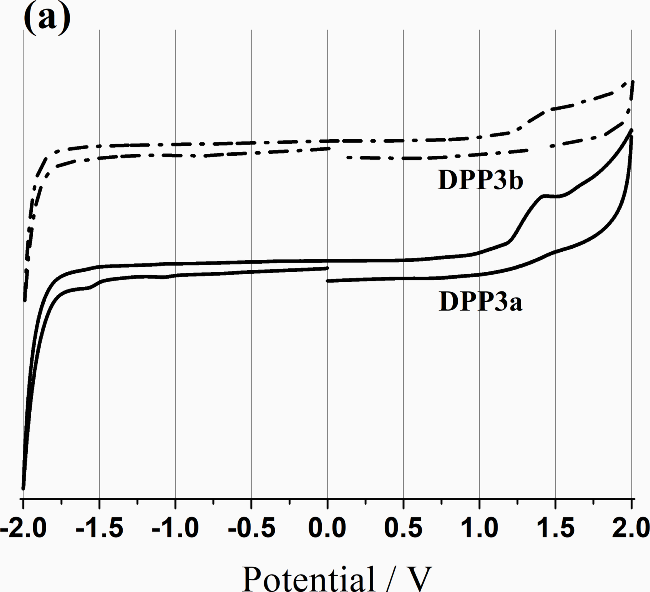
(a)
DPP3b
DPP3a
-2.0
-1.5
-1.0
-0.5
0.0
0.5
1.0
1.5
2.0
Potential / V

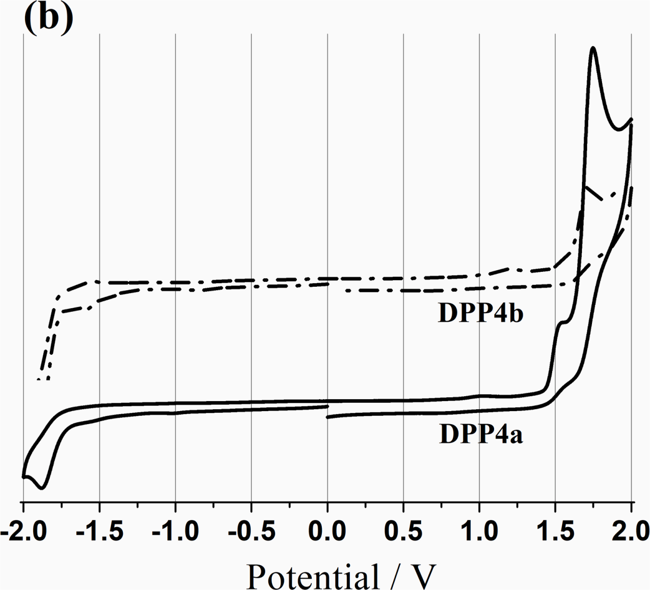
(b)
DPP4b
DPP4a
-2.0
-1.5
-1.0
-0.5
0.0
0.5
1.0
1.5
2.0
Potential / V

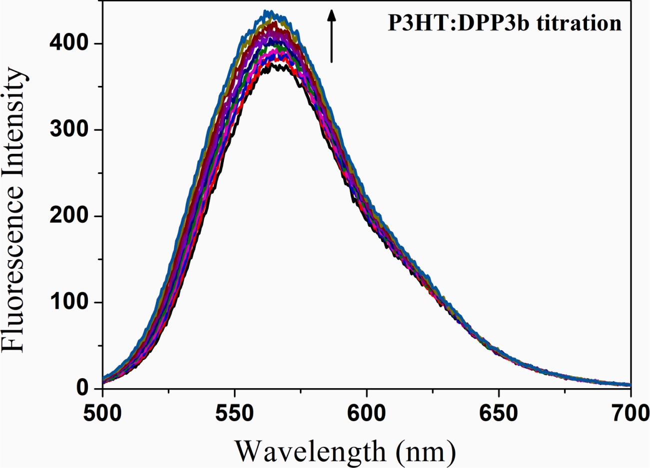
P3HT:DPP3b titration
Fluorescence Intensity
Wavelength (nm)
0
100
200
300
400
500
550
600
650
700

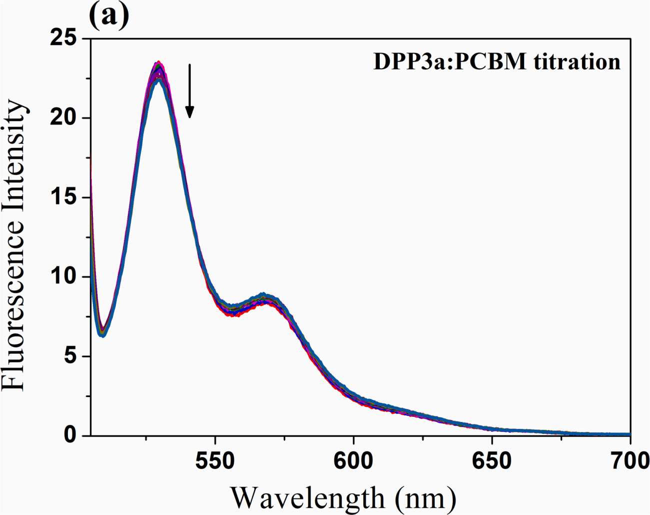
(a)
DPP3a:PCBM titration
Fluorescence Intensity
0
5
10
15
20
25
550
600
650
700
Wavelength (nm)

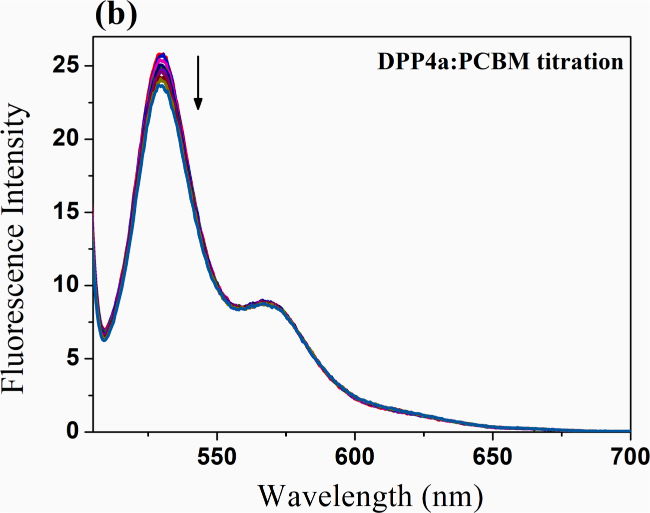
(b)
DPP4a:PCBM titration
Fluorescence Intensity
Wavelength (nm)
0
5
10
15
20
25
550
600
650
700

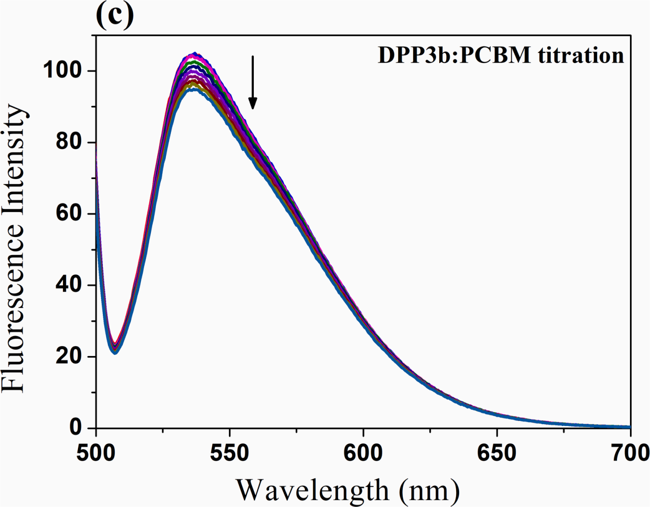
(c)
DPP3b:PCBM titration
Fluorescence Intensity
Wavelength (nm)
0
20
40
60
80
100
500
550
600
650
700

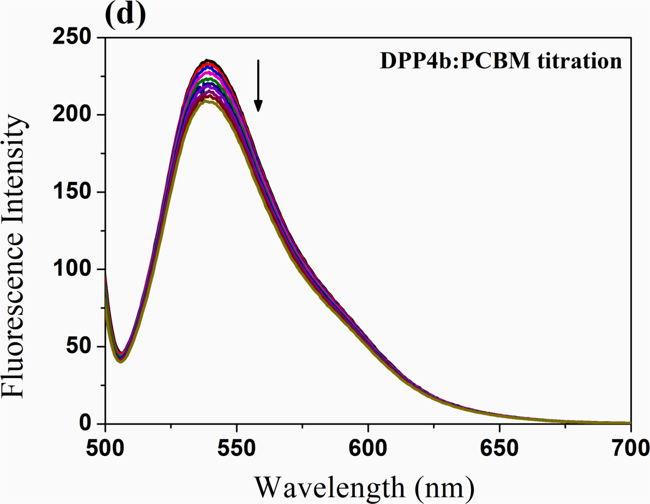
(d)
DPP4b:PCBM titration
Fluorescence Intensity
Wavelength (nm)
0
50
100
150
200
250
500
550
600
650
700

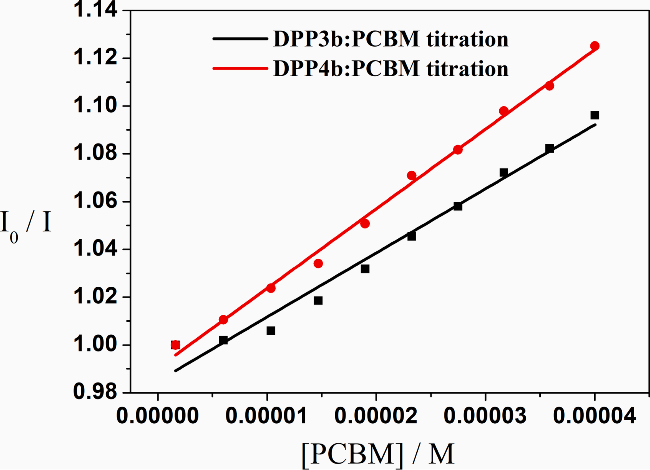
DPP3b:PCBM titration
DPP4b:PCBM titration
1.14
1.12
1.10
1.08
1.06
1.04
1.02
1.00
0.98
I_0 / I
0.00000
0.00001
0.00002
0.00003
0.00004
[PCBM] / M

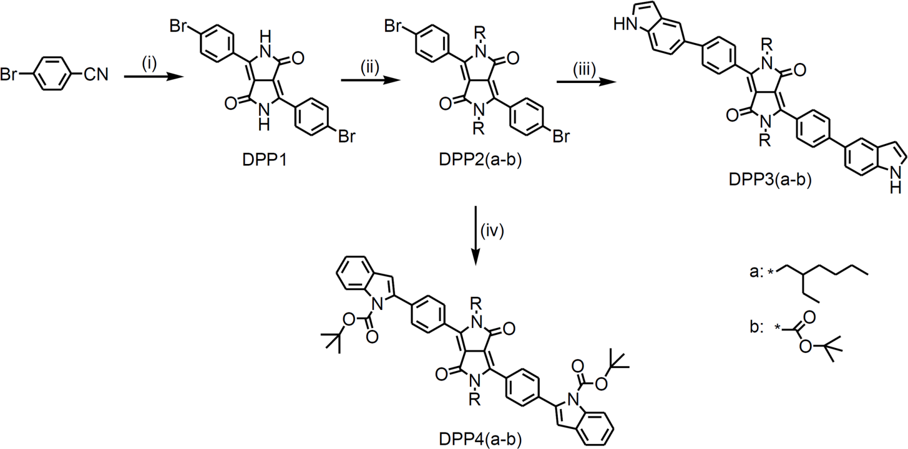
Br
CN
(i)
DPP1
(ii)
DPP2(a-b)
(iii)
DPP3(a-b)
(iv)
DPP4(a-b)
R
a:
b:

Dyes / Solvents	CHCl$_3$			MeCN			Thin Film	
	λ_{abs}	λ_{em}	τ_{f}	λ_{abs}	λ_{em}	τ_{f}	λ_{abs}	λ_{em}
DPP3a	253, 486, 603	557, 598	4.78	255, 480	554, 593	4.07	257, 492	556, 597
DPP3b	270, 305, 470, 600	552, 585	3.57	269, 307, 457	514, 552	5.37	275, 316, 489	600
DPP4a	260, 478, 601	542, 578	6.25	256, 472	540, 575	6.63	315, 486	553, 593
DPP4b	306, 471, 601	552, 593	2.79	300, 459	552, 590	2.82	303, 475	562, 601

Dyes	E^0_{red2} (V)	E^0_{red1} (V)	E^0_{ox1} (V)	E^0_{ox2} (V)	LUMO (eV)	HOMO (eV)	λ_{onset} (nm)	E_g^{opt} (eV)
DPP3a	-	−1.57	1.41	-	−3.45	−5.68	555	2.23
DPP3b	-	−1.59	1.45	-	−3.57	−5.72	577	2.15
DPP4a	−1.88	−1.55	1.52	1.74	−3.51	−5.79	545	2.28
DPP4b	−1.90	−1.59	1.18	1.71	−3.22	−5.45	557	2.23